https://erjm.journals.ekb.eg
ISSN: 1110-1180

DOI: ---------

ERJ
Engineering Research Journal
Faculty of Engineering
Menoufia University

Forced Convection from an Isothermal Circular Cylinder Rotating Steadily in a Cross Stream of Nanofluid

Fathy M. Mahfouz[1], Bilal M. Maher[2], and Mohamed K. Yaseen[2*]

[1]Department of Mechanical Power Eng., Shebin El Kom Faculty of Eng., Menoufia University, Menoufia, Egypt.
[2] Department of Basic Sciences Eng., Shebin El Kom, Faculty of Eng., Menoufia University, Menoufia, Egypt.
(Corresponding author: mohamed_mohamed54@sh-eng.menofia.edu.eg)

ABSTRACT
In this paper forced convection from steady rotating circular cylinder in a cross stream of nanofluid is theoretically investigated. The nanofluid is formed by adding Nanometric particles of copper to water. The flow and energy governing equations are solved using Fourier spectral method. The main influencing parameters on flow and thermal fields are Reynolds number, particles volume fraction and the cylinder speed ratio (peripheral velocity of rotating cylinder/ uniform free stream velocity). The Reynolds number is considered up to 200, the volume fraction of nanoparticles is considered up to 0.05 while the cylinder speed ratio is considered up to 1. The effects of Reynolds number, solid particle volume fraction and cylinder speed ratio on both flow and thermal fields are considered. The study has shown very good agreement with the previous results in the literature for cases of fixed and rotating cylinder in cross stream of a Newtonian fluid. The study has also shown that increasing of volume fraction of nanoparticles increases the heat transfer rate for both fixed and rotating cylinder while increasing the cylinder speed ratio for the given range of parameters is found to decrease heat transfer rate. Also, the study has shown that increasing nanoparticles volume fraction increases drag coefficient for stationary cylinder, while increasing nanoparticles volume fraction decreases drag coefficient for low speed ratios, has no significant effect on lift coefficient, and has a slight increasing effect on Strouhal number. Also, increasing speed ratio α decreases both lift and drag coefficient (for low speed ratios).

Keywords: *Forced Convection - Rotating Cylinder – Nanoliquids – Drag Coefficient.*

1. Introduction

The transmission of flow and heat across a circular cylinder has been the theme of various theoretical and experimental studies. In a number of industrial processes, fluid flow and heat transfer across a circular cylinder is a prevalent phenomenon. Some examples of these processes are: flows containing heat exchanger tubing, chimney stacks, cooling towers, measurement probes and instruments, offshore facilities, and transmission cables,…etc. In the form of von Karman vortex street, instability in the cylinder wake occurs when the number of Reynolds exceeds the range of the critical limit thereof. The essence of this instability of the wake is either absolute or convective. Any initial disruption at any fixed location increases in the event of absolute instability. The wake enters into theframework of a self-sustained oscillation when the nonlinearities have restricted the growth of the disturbance. On the other hand, initial disruption rises over time for convective instability and is transmitted away at the same time, leaving the wake undisturbed. Research shows that the creation of the vortex street in the cylinder wake is owing to absolute disorder in the shape of the symmetric wake mode instantly behind the cylinder wake. Cylinder rotation has a heavy dependency on the thermal boundary layer formation at the cylinder surface, apart from the effect on vortex dynamics and flow characteristics. This is getting a direct control over the rate of heat transfer. Numerous studies dealing with the influence of cylinder rotation on heat transfer phenomena exists.

Conventional fluids such as air and water have been used in several of studies. However, relative to metals and even metal oxides, such conventional heat transfer fluids have inherently poor thermal conductivity. Low thermal conductivity is a primary limitation in the development of energy-efficient heat transfer fluids that are required in many industrial

applications. Industries have concentrated on the production of modern fluids with better thermal properties, such as nanoliquids, because of growing global competition and the essential position of energy. Owing to its excellent thermo-physical behavior, increased stability, and homogeneity, nanoscale particle suspensions (nanoliquids) have often been used as an effective heat transfer medium in recent times. Nanoliquids are considered one phase flow which are formed of base fluid (include water and organic liquids) and solid metallic or non-metallic particles with a particle size below 100 nm on average [1–3]. Also with a limited amount of particle volume fraction, the higher conductivity of the nanoparticle presence in the base fluid leads to thermal conductivity improvement of the nanoliquid.

A review of the preceding published papers-as far as the writer of this research knows-concerning the influence of the rotation of a circular cylinder on the behavior of the fluid flow and on the behavior of the heat transfer shows that numerous experimental procedures and computation methods has been carried out in to analyze the influence of rotation on the behavior of flow and heat transfer across a circular cylinder.

Prandtl [4] conducted the earliest known research on fluid flow past a cylinder rotating in a free stream.

Badr and Dennis [5] analyzed the effect of the rotation rate α for Reynolds number Re ≥200 on the flow past impulsive started rotating cylinder, the research concerned with the initial logarithmic function of Reynolds number. The authors concluded that increasing the rate α increases the lift force and decreases the mean drag.

The research of Badr and Dennis [6] is considered one of the first numerical investigations deals with forced convection deduced from a cylinder rotating in a cross of laminar fluid flow at Re =100 and $\alpha \leq 4$. The authors observed that the flow and thermal fields are highly influenced by the speed ratio in the recognized range. Also, they mentioned that owing to the presence of a revolving fluid layer that separates the cylinder from the main stream, the average heat transfer coefficient tends to decrease as the speed ratio increases.

Ingham and Tang [7] investigated the influence of a speed ratio $\alpha \leq 3$ and moderate Reynolds number Re ≤ 47. They mentioned that for small values of α the streamlines occur only very closely to the cylinder, but they appear in larger and larger regions as α rises. In addition, the authors mentioned that as α grows, the cylinder rotates with an increasing amount of fluid around it. Also they mentioned that the speed ratio has been used in several of the above investigations, restricted to just $\alpha \leq 3$. Also, the authors clarified that several numerical methods of research has been executed which shows that the flow appears unstable for a specific range of speed ratio and activates vortex shedding.

Stojkovic et al.[8] examined laminar flow past a rotating circular cylinder. In addition, they also extended their numerical computations for one characteristics Reynolds number of 100 and at very high speed ratios, $\alpha \leq 12$. Their computational studies showed that at Re = 100, vortex shedding is observed for a narrow range of rotation rates $4.8 \leq \alpha \leq 5.15$.

Stojkovic et al. [9] extended their analysis in the Reynolds number range $60 \leq Re \leq 200$ and at speed ratio$0 \leq \alpha \leq 6$. Second vortex shedding mode on the flow, depending upon the magnitude of Reynolds number in the range of speed ratios$4.35 \leq \alpha \leq 5.45$, appeared.

Mittal and Kumar [10] analyzed flow past cylinder for Re = 200 for different speed ratios $0 \leq \alpha \leq 5$. They found also that in the range of $0 \leq \alpha \leq 1.9$ von Karman street is observed in the wake behind the cylinder. The vortex street is deflected away from the middle line for non-zero α. The wake is narrower and with an increase in speed ratio, the amount of Strouhal for vortex shedding decreases. Also, they deduced that the vorticity produced on the cylinder surface is dragged along with it for high α. The positive and negative vorticity appear as tightly wound spirals. The flow remains stable for $1.91 \leq \alpha \leq 4.35$ but loses its stability again for $\alpha \sim 4{:}35$.

Sanitjai, Surachai and Goldstein [11] analyzed the forced convection from a circular cylinder in cross flow of air and liquids. They reported that for subcritical flow, three flow regions around the cylinder are indicated by the local heat transfer measurement: laminar boundary layer area, shear layer region reattachment, and periodic vortex flow region.

Abdella et al. [12] studied the forced convection from a shear flow across a rotating cylinder using approximate analytic solution via series expansion of the scaled boundary layer equations in terms of an appropriate boundary layer variable. Not only for the initial phases of issues relating small and moderate Reynolds numbers, but also for moderate and large periods for sufficiently large Reynolds number problems, the stated solution was correct.

Paramane and Sharma[13] analyzed with numerical techniques the effect of the rotation rate on the flow and heat transfer through a rotating cylinder in the range of $0 \leq \alpha \leq 6$ and $20 \leq Re \leq 160$, and they concluded that rotation could be used as a strategy for drag reduction and heat transfer suppression.

Paramane and Sharma [14] concluded that at higher rotational velocity, the Nusselt number is almost

independent of Reynolds number and thermal boundary conditions as the heat transfer near cylinder surface is limited to conduction only.

Khelili et al. [15] used copper-water nanofluid in their study for forced convection flow over steady rotating cylinder for low Reynolds number $5 \leq Re \leq 40$ and speed ratiovarying from 0 to 5 with concentration $0 \leq \varphi \leq 0.05$. And they reported that with increasing Reynolds number and increasing speed ratio, heat transfer suppression due to rotation increases. Also, the suppression of heat transfer is not improved due to the addition of nanoparticles through the base fluid. A downward drag coefficient is also considered to be due to rotation, which, with increasing speed ratio, decreases monotonically. As a drag reduction strategy, rotation can thus be used. In addition, as the speed ratio increases and as the Reynolds number increases, the average Nusselt number is found to decrease. Khelili et al. [16] extended their study to $50 \leq Re \leq 300$ and stated that by inserting nanoparticles into the base fluid, the vorticity, pressure coefficient, and recirculation duration are increased.

Hussain, et al. [17] analyzed and discussed the forced convection heat transfer and hydrodynamic forces with nanofluid flow over rotating cylinder using finite element method in the range of $10 \leq Re \leq 200$ and volume fraction of nanoparticles $0 \leq \varphi \leq 0.04$. They reported that the cylinder's clockwise rotation causes the fluid to travel above the cylinder while the fluid in the anti-clockwise case moves below the cylinder. Moreover, an increase in the nanoparticles volume fraction enhances the average Nusselt number and decreases both of the lift and drag coefficients.

Korib et al. [18] concluded from their study to the steady flow-field and heat transfer through a copper-water nanofluid around a circular cylinder, under the influence of both the standard thermal boundary conditions, i.e., uniform heat flux and constant wall temperature that local and average Nusselt figures were improved by adding nanoparticles to the base fluid at a given Reynolds number. Moreover, higher values of the average Nusselt number are provided by the UHF boundary condition. Despite a number of studies published in the literature on convective heat transfer of nanoliquids, it has largely been ignored to investigate forced convective flow and heat transfer past a rotating circular cylinder using nanofluid as the operating medium. In designing many heat transfer devices used in modern industry, however, this issue has important applications. Nevertheless, few studies have recently been published on forced and mixed convective heat transfer of nanoliquids past circular cylinders.

1.2. Aim of the Research

Since there is a lack of analysis of nanoliquid activity around the cylinder and because of its broad application, the forced convection heat transfer from a constant wall temperature rotating circular cylinder is investigated using Fourier spectral method. The study considers the effect of Reynolds number, nanoparticle volume fraction, and speed ratio on Strouhal number, hydrodynamics forces and forced convection associated with the cross flow of nanofluid over circular cylinder of a horizontal axis. In engineering applications, the cross section of the cylinder might be selected as circle or elliptic. In most applications circular cylinders are widely used. The selection of the cylinder shape needs more investigations to optimize the objectives of the problem. The cylinder of circular cross section shape is selected in the present work. The solid cylinders of elliptic cross section are under investigation in many preceding's [19–21] and recent investigations.

2. Formulation of the Problem

The physical domain under consideration is shown in Fig.1 where laminar flow of an incompressible nanofluid with uniform velocity U_∞ and temperature T_∞ passes across an infinitely long (in *z*-direction) horizontal circular isothermal cylinder of radius R. The cylinder surface is heated and kept at constant temperature T_S ($T_S > T_\infty$). In this analysis the thermo-physical properties of the streaming nanofluid are independent of temperature, also viscous dissipation effects are negligible.

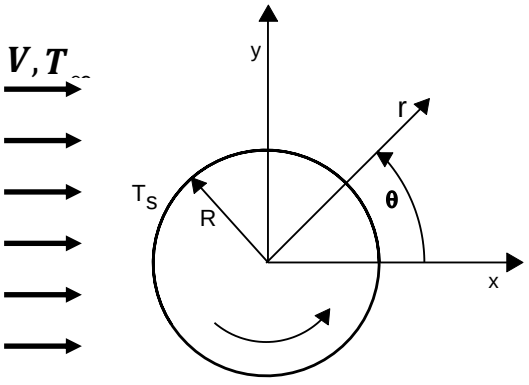

Figure 1- Physical domain and coordinate system

2.1 The Governing Equations

Considering cylindrical coordinate system (r,θ,z) where $0 \leq \theta \leq 360$ is measured counterclockwise from the rearmost point of the cylinder surface. r is the radial coordinate extended from the origin of the cylinder to the layer where the effects of the cylinder on flow and thermal fields vanish. Since the cylinder

is very long (in *z*-direction) the flow is assumed to be two dimensional. Under the suggested the conservation equations of mass, momentum and energy are expressed as follows:

Continuity equation:

$$\frac{1}{r}\frac{\partial(r\,U_r)}{\partial r}+\frac{1}{r}\frac{\partial(U_\theta)}{\partial\theta}=0 \quad (1)$$

Momentum equation in r direction:

$$\frac{\partial U_r}{\partial t}+U_r\frac{\partial U_r}{\partial r}+\frac{U_\theta}{r}\frac{\partial U_r}{\partial\theta}-\frac{(U_\theta)^2}{r}=-\frac{1}{\rho}\frac{\partial P}{\partial r}+\nu\left[\nabla^2U_r-\frac{U_r}{r^2}-\frac{2}{r^2}\frac{\partial U_\theta}{\partial\theta}\right] \quad (2)$$

Momentum equation in θ direction:

$$\frac{\partial U_\theta}{\partial t}+U_r\frac{\partial U_\theta}{\partial r}+\frac{U_\theta}{r}\frac{\partial U_\theta}{\partial\theta}-\frac{U_\theta U_r}{r}=-\frac{1}{\rho\,r}\frac{\partial P}{\partial\theta}+\nu\left[\nabla^2U_\theta-\frac{U_\theta}{r^2}+\frac{2}{r^2}\frac{\partial U_r}{\partial\theta}\right] \quad (3)$$

Energy equation:

$$\frac{\partial T}{\partial t}+U_r\frac{\partial T}{\partial r}+\frac{U_\theta}{r}\frac{\partial T}{\partial\theta}=\frac{K}{\rho\,C_p}\nabla^2\mathrm{T} \quad (4)$$

Where, $\nabla^2=\frac{1}{r}\frac{\partial}{\partial r}+\frac{\partial^2}{\partial r^2}+\frac{1}{r^2}\frac{\partial^2}{\partial\theta^2}$

Reducing the number of variables by introducing the stream function defined by the velocity components $U_r=\frac{1}{r}\frac{\partial\psi}{\partial\theta}$, $U_\theta=-\frac{\partial\psi}{\partial r}$ and by eliminating the pressure gradient between equation (2) and equation (3), the continuity equation is verified and the set of equations (2-4) are reduced to the simplified forms:

$$\frac{\partial\Omega}{\partial t}+\frac{1}{r}\frac{\partial\psi}{\partial\theta}\frac{\partial\Omega}{\partial r}-\frac{1}{r}\frac{\partial\psi}{\partial r}\frac{\partial\Omega}{\partial\theta}=\nu\nabla^2\Omega \quad (5)$$

$$\frac{\partial\mathrm{T}}{\partial t}+\frac{1}{r}\frac{\partial\psi}{\partial\theta}\frac{\partial\mathrm{T}}{\partial r}-\frac{1}{r}\frac{\partial\psi}{\partial r}\frac{\partial\mathrm{T}}{\partial\theta}=\frac{K}{\rho\,C_p}\nabla^2 \quad (6)$$

Where, Ω is the flow vorticity defined as $\Omega=\frac{\partial U_\theta}{\partial r}+\frac{U_\theta}{r}-\frac{1}{r}\frac{\partial U_r}{\partial\theta}$ and can be written in terms of the stream function as $\Omega=-\nabla^2\psi$. The boundary conditions of the problem under consideration are the no-slip condition, the impermeability condition and isothermal condition on the cylinder surface together with the free stream conditions which is considered very faraway from the cylinder surface. These conditions can be expressed as follows

At the cylinder surface, $r=R$

$\psi=\frac{\partial\psi}{\partial\theta}=0$, $\frac{\partial\psi}{\partial r}=-U_s$, and $T=T_s$ (7-a)

As $r\to\infty$,

$\frac{\partial\psi}{\partial\theta}=-r\,V\cos\theta$, $\frac{\partial\psi}{\partial\theta}=-V\sin\theta$, $\Omega\to0$,

and $T=T_\infty$ (7-b)

Introducing the following dimensionless parameters:

$$r'=\frac{r}{R},t'=\frac{t\,V}{R},\psi'=\frac{\psi}{R\,V},\Omega'=-\Omega\frac{R}{V},$$

$$\phi=\frac{T-T_\infty}{T_s-T_\infty},Re=\frac{2\,R\,V}{\nu},Pr=\frac{\mu\,C_p}{K}$$

and using the modified polar coordinates (ξ,θ) where $\xi=\ln r$, and dropping the primes, the set of equations (5-6) and the boundary conditions (7) become:

$$e^{2\xi}\frac{\partial\Omega}{\partial t}=\frac{2}{Re}\left[\frac{\partial^2\Omega}{\partial\xi^2}+\frac{\partial^2\Omega}{\partial\theta^2}\right]-\frac{\partial\psi}{\partial\theta}\frac{\partial\Omega}{\partial\xi}+\frac{\partial\psi}{\partial\xi}\frac{\partial\Omega}{\partial\theta} \quad (8)$$

$$e^{2\xi}\Omega=\frac{\partial^2\psi}{\partial\xi^2}+\frac{\partial^2\psi}{\partial\theta^2} \quad (9)$$

$$e^{2\xi}\frac{\partial\phi}{\partial t}=\frac{2}{Re\,Pe}\left[\frac{\partial^2\phi}{\partial\xi^2}+\frac{\partial^2\phi}{\partial\theta^2}\right]-\frac{\partial\psi}{\partial\theta}\frac{\partial\phi}{\partial\xi}+\frac{\partial\psi}{\partial\xi}\frac{\partial\phi}{\partial\theta} \quad (10)$$

Associated with the boundary conditions:

At $\xi=0$, $\psi=\frac{\psi\partial}{\partial\theta}=0$, $\frac{\psi\partial}{\xi\partial}=-\alpha$, and $\phi=1$ (11-a)

As $\xi\to\infty$, $\frac{\partial\psi}{\partial\theta}=e^{\xi}\cos\theta$, $\frac{\partial\psi}{\partial\xi}=e^{\xi}\sin\theta$, $\Omega=0$, and $\phi=0$ (11-b)

2.2 The Thermo-Physical Properties of a Nanoliquid

The density of the dispersed liquid ρ_{nf} is expressed in terms of the nanoparticles volume concentration φ, liquid density ρ_f, and particle density ρ_p, related by the formula [22]

$$\rho_{nf}=(1-\varphi)\,\rho_f+\varphi\,\rho_p \quad (12)$$

The specific heat of a nanofluid is calculated by using energy balance equation mentioned in Khelili et al. [16]

$$(\rho\,C_p)_{nf}=(1-\varphi)(\rho\,C_p)_f+\varphi(\rho\,C_p)_p \quad (13)$$

where the ratio φ is written as mentioned in [16]

$$\varphi=\frac{Volume\ of\ nanoparticles}{Total\ volume\ of\ nanofluid} \quad (14)$$

The effective thermal conductivity of a nanofluid is approximated by Maxwell-Garnett model. Depending on this model Yu and Choi [23] suggested a formula for a suspension of spherical nanoparticles in the base fluid which takes the form; as it is

$$K_{nf} = K_f \left[\frac{(K_p+2K_f)-2\varphi(K_f-K_p)}{(K_p+2K_f)+\varphi(K_f-K_p)}\right] \quad (15)$$

The effective dynamic viscosity of a nanofluid can be calculated by using Brinkman formula mentioned in [24] which takes the form

$$\mu_{nf} = \frac{\mu_f}{(1-\varphi)^{2.5}} \quad (16)$$

The effective Reynolds number Re and Prandtl number Pr of a nanofluid are related to the properties of the base fluid and the properties of nanoparticles according to the relations [15]:

$$Re = Re_f \frac{\rho_{nf}}{\rho_f} \frac{\mu_f}{\mu_{nf}} \quad (17)$$

$$Pr = Pr_f \frac{\mu_{nf}}{\mu_f} \frac{Cp_{nf}}{Cp_{nf}} \frac{K_f}{K_{nf}} \quad (18)$$

The selection of the best nanoparticles requires dynamic and mathematical analysis to investigate the effects of different types. No investigations have been done to compare the effect of different kinds of nanoparticles (To the best knowledge of the author). For minute details of the types of the nanoparticles reference may be made to [25] and [26]. The presented analysis includes only one nanoliquid (water + Cu) under consideration. Copper is chosen for its effective heat conduction properties. The thermo-physical properties of the base liquid (water) and the nanoparticles (copper) are listed in Table. 1 as mentioned in [16].

Where, ρ [kg/m^3], K [W/m.º K], C_p [J/kg.º K], μ [kg/m.s], and Pr is dimensionless.

Table 1- Thermo-physical properties of nanoparticles and base liquid.

Properties	ρ	K	C_p	μ*10^{-3}	Pr
Water	997.1	0.613	4179	1.003	7
Copper	8933	400	385	---	---

3. The Method of Solution

Many common methods have been investigated to solve the problem under investigation, Fourier spectral method is one of them. This method is selected because it is convenient, has simple procedures and accurate results. In the view of Fourier spectral method, the dimensionless stream function ψ, vorticity Ω, and temperature ϕ take the form [27]:

$$\psi(\xi,\theta,t) = \frac{1}{2} F_o(\xi,t) + \sum_{n=1}^{N}[f_n(\xi,t)\sin n\theta + F_n(\xi,t)\cos n\theta] \quad (19\text{-a})$$

$$\Omega(\xi,\theta,t) = \frac{1}{2} G_o(\xi,t) + \sum_{n=1}^{N}[g_n(\xi,t)\sin n\theta + G_n(\xi,t)\cos n\theta] \quad (19\text{-b})$$

$$\phi(\xi,\theta,t) = \frac{1}{2} H_o(\xi,t) + \sum_{n=1}^{N}[h_n(\xi,t)\sin n\theta + H_n(\xi,t)\cos n\theta] \quad (19\text{-c})$$

Where F_o, f_n , F_n , G_o, g_n , G_n, H_o, h_n , H_n are Fourier coefficients and N denotes the number of terms in the series. Referring to the work of Badr and Dennis [28] , and also referring to the work of Mahfouz and Badr [29], the set of equations (8-10) could be integrated from $\theta = 0$ to $\theta = 2\pi$ after substituting with equation (19), the following system of partial differential equations in terms of Fourier series coefficients is found to be as follows:

$$\frac{\partial^2 F_o}{\partial \xi^2} = e^{2\xi} G_o \quad (20\text{-a})$$

$$\frac{\partial^2 f_n}{\partial \xi^2} - n^2 f_n = e^{2\xi} g_n \quad (20\text{-b})$$

$$\frac{\partial^2 F_n}{\partial \xi^2} - n^2 F_n = e^{2\xi} G_n \quad (20\text{-c})$$

$$e^{2\xi}\frac{\partial G_o}{\partial t} = \frac{2}{Re}\frac{\partial^2 G_o}{\partial \xi^2} + S_o \quad (21\text{-a})$$

$$e^{2\xi}\frac{\partial g_n}{\partial t} = \frac{2}{Re}\left[\frac{\partial^2 g_n}{\partial \xi^2} - n^2 g_n\right] + \frac{n}{2} F_n \frac{\partial G_o}{\partial \xi} - \frac{n}{2} G_n \frac{\partial F_o}{\partial \xi} + \frac{1}{2} S_{n1} \quad (21\text{-b})$$

$$e^{2\xi}\frac{\partial G_n}{\partial t} = \frac{2}{Re}\left[\frac{\partial^2 G_n}{\partial \xi^2} - n^2 G_n\right] - \frac{n}{2} f_n \frac{\partial G_o}{\partial \xi} + \frac{n}{2} g_n \frac{\partial F_o}{\partial \xi} + \frac{1}{2} S_{n2} \quad (21\text{-c})$$

$$e^{2\xi}\frac{\partial H_o}{\partial t} = \frac{2}{Re\ Pr}\frac{\partial^2 H_o}{\partial \xi^2} + Z_o \quad (22\text{-a})$$

$$e^{2\xi}\frac{\partial h_n}{\partial t} = \frac{2}{Re\ Pr}\left[\frac{\partial^2 h_n}{\partial \xi^2} - n^2 h_n\right] + \frac{n}{2} F_n \frac{\partial H_o}{\partial \xi} - \frac{n}{2} H_n \frac{\partial F_o}{\partial \xi} + \frac{1}{2} Z_{n1} \quad (22\text{-b})$$

$$e^{2\xi}\frac{\partial H_n}{\partial t} = \frac{2}{Re\ Pr}\left[\frac{\partial^2 H_n}{\partial \xi^2} - n^2 H_n\right] - \frac{n}{2} f_n \frac{\partial H_o}{\partial \xi} + \frac{n}{2} h_n \frac{\partial F_o}{\partial \xi} + \frac{1}{2} Z_{n2} \quad (22\text{-c})$$

where, S_o, S_{n1}, S_{n2}, Z_o, Z_{n1}, Z_{n2} are functions in ξ and t (see appendix). Equations (20-a)-(22-c) define a set of (6N+3) differential equations that should be

solved at every time step to get the flow stream ψ, vorticity Ω, and dimensionless temperature ϕ. Also, the boundary conditions of the problem in terms of Fourier series coefficients are found to be:

$$\text{At } \xi = 0,\ F_o = f_n = F_n = \frac{\partial F_n}{\partial \xi} = \frac{\partial f_n}{\partial \xi} = 0,\ \frac{\partial F_o}{\partial \xi} = -2\alpha,\ H_o = 2, \text{ and } h_n = H_n = 0 \quad (23\text{-a})$$

$$\text{As } \xi \to \infty, F_o = F_n = \frac{\partial F_n}{\partial \xi} = \frac{\partial F_o}{\partial \xi} = 0,\ f_n = e^{\xi}\delta_{1,n},\ \frac{\partial f_n}{\partial \xi} = e^{\xi}\delta_{1,n}, G_o = g_n = G_n = 0, \text{ and } H_o = h_n = H_n = 0 \quad (23\text{-b})$$

The integral boundary conditions can be deduced by integrating both sides of equations (20.1), (20.2), and (20.3) with respect to ξ from $\xi = 0$ to $\xi = \infty$ and by using boundary conditions equation (23). These integrals are used at every time step to calculate the functions G_o, g_n, G_n at the cylinder surface when $\xi = 0$ .The deduced integrals of the boundary conditions are then used to calculate the vorticity distribution on the cylinder surface to a certain accuracy.

$$\int_0^{\infty} e^{2\xi} G_o(\xi, t)\, d\xi = 2\alpha \quad (24\text{-a})$$

$$\int_0^{\infty} e^{(2-n)\xi} g_n(\xi, t)\, d\xi = 2\delta_{1,n} \quad (24\text{-b})$$

$$\int_0^{\infty} e^{(2-n)\xi} G_n(\xi, t)\, d\xi = 0 \quad (24\text{-c})$$

The rest of the details of Fourier spectral method and Crank-Niclson method are similar to that used in references [28–30]. For brevity, these details are not repeated. Form the numerical procedures used for obtaining the stream function ψ, vorticity Ω, and temperature ϕ, the final formulations of drag coefficient, lift coefficient, and Nusselt number are obtained as follows:

3.1 Drag Coefficient

The total drag coefficient is written

$$C_D = C_{DP} + C_{DF} \quad (25)$$

The deduced drag coefficient in terms of Fourier coefficients takes the form

$$C_D = \frac{2\pi}{Re}\left[g_1(0,t) - \left(\frac{\partial g_1}{\partial \xi}\right)_{\xi=0}\right] \quad (26)$$

3.2 Lift Coefficient

The total lift coefficient is written

$$C_L = C_{LP} + C_{LF} \quad (27)$$

The deduced lift coefficient in terms of Fourier coefficients takes the form

$$C_L = -\frac{2\pi}{Re}\left[G_1(0,t) - \left(\frac{\partial G_1}{\partial \xi}\right)_{\xi=0}\right] \quad (28)$$

3.3 Nusselt Number

Local and average Nusselt numbers are defined as follows:

$$Nu = \frac{h\,d}{K} \text{ and } Nu_{avg} = \frac{\bar{h}\,d}{K} \quad (29)$$

where, h and $\bar{h}$ are the local and the average heat transfer coefficients. These coefficients can be expressed in terms of Fourier coefficients as follows [27]:

$$Nu = -2\left(\frac{\partial \phi}{\partial \xi}\right)_{\xi=0} = -\left[\frac{\partial H_o}{\partial \xi} + 2\sum_{n=1}^{N} \frac{\partial h_n}{\partial \xi}\sin n\theta + \frac{\partial H_n}{\partial \xi}\cos n\theta\right]_{\xi=0} \quad (30)$$

$$Nu_{avg} = -\left(\frac{\partial H_o}{\partial \xi}\right)_{\xi=0} \quad (31)$$

4. Results and Discussion.

4.1 Validation of the Results

The problem of forced convection from a fixed and rotating cylinder in Newtonian fluid flow is first discussed and the obtained results are compared with the available numerical and experimental results in order to judge the validity of the mathematical model as well as the numerical technique. These comparisons are shown in Fig. 2, Fig.3 and Fig.4. In these figures the solid and dashed lines in the figure legend represent the present results while symbols in the same legend represent the corresponding results in the literature. Fig. 2 show the evolution with time of the radial velocity on the symmetry axis θ=0 behind a fixed cylinder for Re=550 and comparison with the corresponding results of Ta PhoucLoc [31].

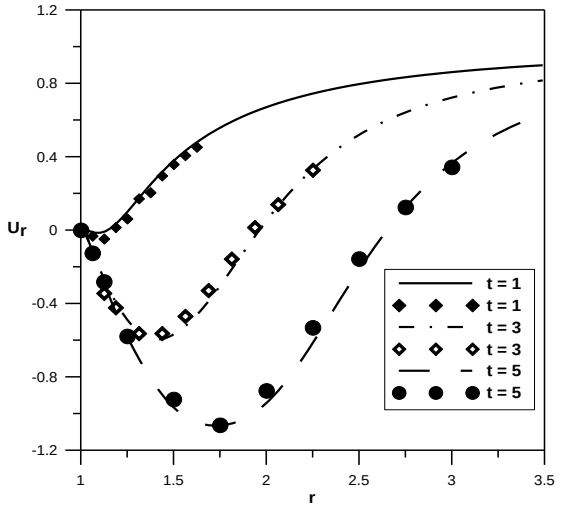

Figure 2- Evaluation of instantaneous radial velocity on the symmetry axis behind the cylinder when Re = 550 and comparison with the corresponding results of Ta PhoucLoc [31]..

On the other hand, the present predictions for the initial flow development over the rotating cylinder are compared with that obtained from the pioneer experimental study of Coutanceau M. and Menard [32]. The comparison is carried out for two speed ratios (rotating speed/free stream velocity) α=0.5, α=1 when Re= 200. The velocity components along line θ=0 are well compared with the experimental one as shown in Fig.3 and Fig.4 respectively.

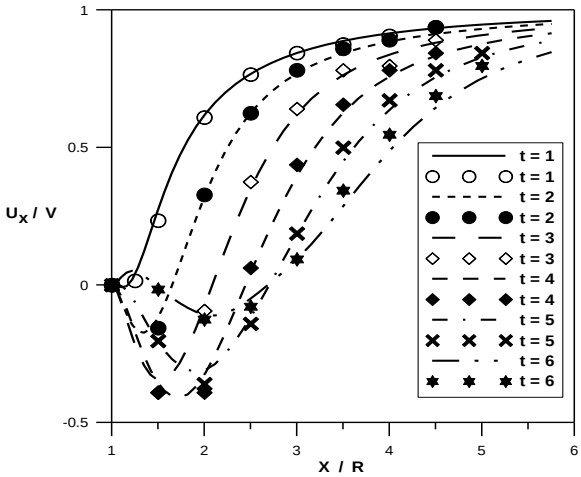

Figure 3.1- Time development of x-velocity component along x-axis when Re=200, α=0.5.

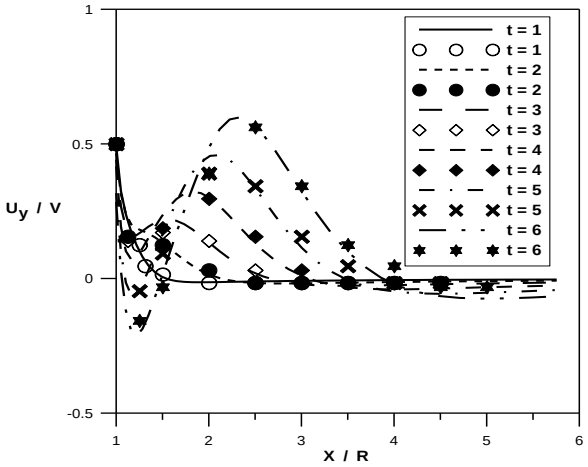

Figure 3.2- Time development of y-velocity component along x-axis when Re=200, α=0.5.

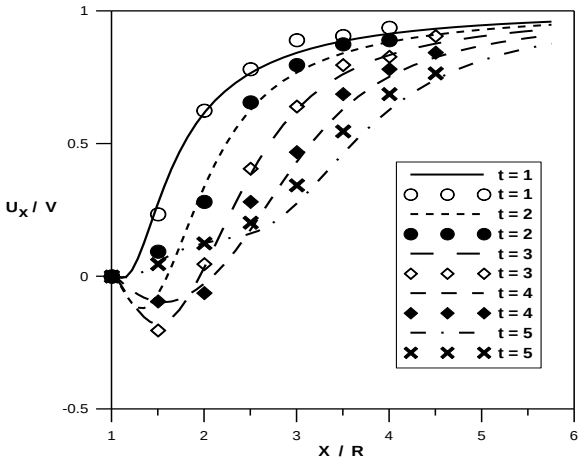

Figure 4.1- Time development of x-velocity component along x-axis when Re=200, α=1

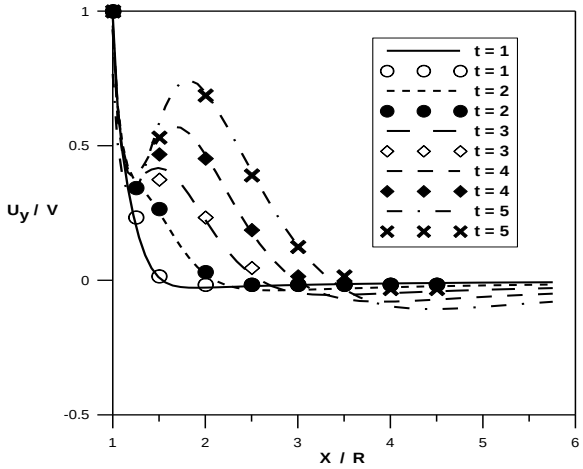

Figure 4.2- Time development of y-velocity =1.αcomponent along x-axis when Re=200,

The predicted values of the C_D and the Nu_{avg} from the present investigation compare well with the corresponding values from preceding published papers as indicated in table 2.

Table 2- The predicted C_D and Nu_{avg} at different Re compared with previous researches for the case of stationary cylinder.

Re	C_D			Nu_{avg} (Pr=0.7)		
	Present Study	Ref. [33]	Ref. [34]	Present Study	Ref. [34]	Range of Ref. [35–39]
80	1.386267	1.4	1.33	4.819263	4.8	4.59-4.95
100	1.372249	1.38	1.32	5.485895	5.25	4.769-5.52
200	1.595073	1.32	1.31	8.368245	7.8	6.67-7.63

The flow past circular cylinder with an impulsive start when Re = 200 with α = 0.5 is computed. The numerical results of the instantaneous streamlines for the same variables are compared with the numerical and experimental results of Badr and Dennis[28]. The compared graphs are illustrated in Fig.5. Excellent agreement is observed between the corresponding patterns for every time step.

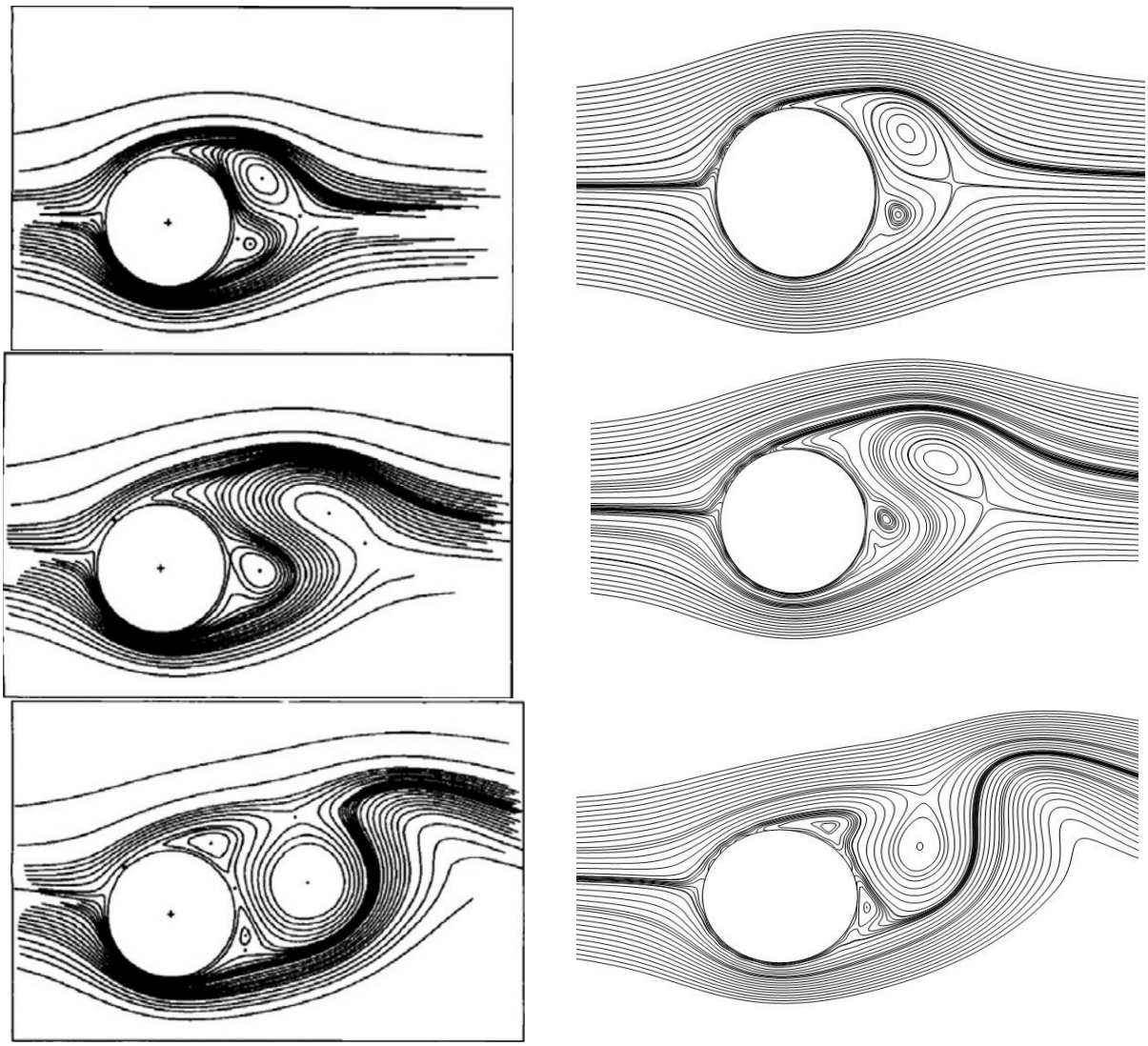

Figure 5- Comparative patterns between instantaneous stream lines of the present results(right side) and preceding results [28] (left side) when: t=3,t=6,t=9.

4.2 Results and Discussion

The first section of the results shows the effect of the nanoparticles volume fraction on both average Nusselt number and drag coefficient in case of stationary cylinder with no vortex shedding. Table 3 reports the effect of φ in the range of $0 \leq \varphi \leq 0.05$, and for the base liquid Reynolds number Re=80, Re=100 and Re= 200 respectively. From Table 3, for the case of stationary cylinder, increasing Re increases Nu_{avg} and increases C_D. For constant Re, increasing φ has significant increasing effect on Nu_{avg} and C_D is increased.

Table 3- The effects of Re and φ on Nu_{avg} and on C_D for fixed cylinder at t=50.

Re	φ	Nu_{avg}	C_D
80	0.00	11.81822	1.386267
	0.01	12.0816	1.380219
	0.02	12.31543	1.376216
	0.03	12.5224	1.373779
	0.05	12.86429	1.372155
100	0.00	13.31908	1.372249
	0.01	13.61183	1.373797
	0.02	13.86909	1.376835
	0.03	14.09452	1.380916
	0.05	14.4611	1.390869
200	0.00	18.27027	1.595073
	0.01	18.53116	1.631761
	0.02	18.74608	1.666466
	0.03	18.926	1.698877
	0.05	19.22554	1.75652

In the next, section the effect of φ on the flow characteristics around the side surface of a stationary cylinder with vortex shedding is discussed. In the numerical scheme, the vortex shedding process is triggered by inducing rotational oscillation to the cylinder for only one complete cycle (at t=40) and stopping it afterwards. The Karman vortex street is developed with vortices being shed alternately from the upper and the lower surfaces of the cylinder. The frequency of the vortex shedding is computed from either the periodic variation of the velocity at any point in the wake or from the time variation of the induced oscillating lift force [40]. The dimensionless frequency of the vortex shedding is expressed as the natural Strouhal number $St = f_o\, d\, /U_\infty$ where f_o is the frequency of the vortex shedding. In table 4 the effect of φ on natural St, Nu_{avg}, and C_D when Re =100 and at α = 0.5 are tabulated. A good agreement is observed between the current predicted value of natural St at φ=0 and the reported value of Roshko [41] which is found to be St=0.165. Increasing φ has a slight increasing on St, also it increases Nu_{avg}. On the hand, C_D is increased by increasing the ratio φ. The instantaneous lift of this case is illustrated in Fig. 6 which shows that the amplitude of C_L increases by increasing φ.

Table 4- The effects of φ on St, Nu_{avg}, and C_D for fixed cylinder with vortex shedding at Re =100, α = 0.5 and t = 250.

φ	St	Nu_{avg}	C_D
0.00	0.1694	15.24793	1.743077
0.01	0.1739	15.26634	1.758295
0.02	0.1793	15.82998	1.731066
0.03	0.1834	16.22772	1.754121
0.05	0.1941	16.71322	1.786122

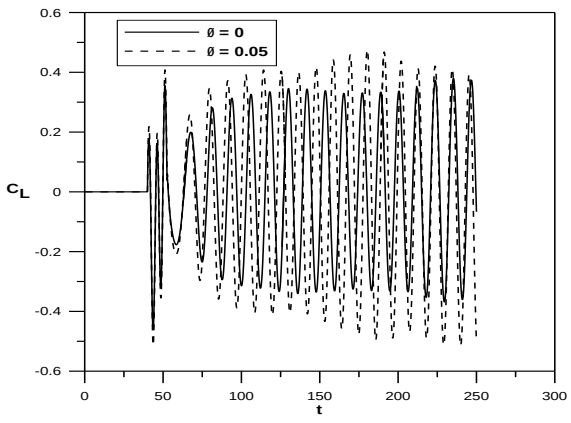

Figure 6- The effect of φ on instantaneous C_L with time when Re=100.

The next section of the results discusses the case of steadily rotating cylinder, the effects of both speed ratio α and the ratio φ on different flow variables are discussed and reported at specified Re. For Re =100 table 5 illustrates the effects of φ on Nu_{avg}, C_L and C_D at α = 0.5 when t = 100.

Table 5- The effects of φ on Nu_{avg}, C_D and C_L when Re=100 and α =0.5, t=100.

φ	Nu_{avg}	C_L	C_D
0.00	11.8199	-.7835838	1.584722
0.01	11.99775	-.6042376	1.562215
0.02	12.27037	-.4456884	1.556728
0.03	12.53907	-.3491957	1.566976
0.05	13.217	-.3541693	1.599355

Table 5 illustrates that increasing φ slightly affects St, also increasing φ has a significant effect that increases the rate of heat transfer Nu_{avg}. In case of a rotating cylinder increasing the ratio φ decreaes C_D.

Fig. 7 illustrates the instantaneous C_L with different values of the ratio φ. Also, one can observe that the effect of φ on St is not significant, increasing φ has no significant effect on the amplitude of C_L.

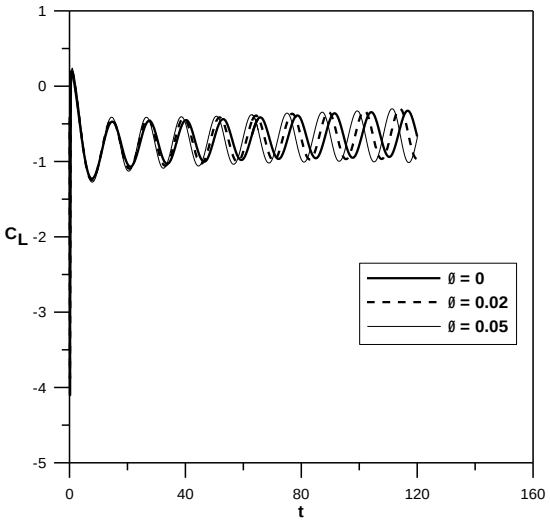

Figure 7- Instantaneous C_L at Re=100 and α = 0.5 with different values of φ.

Fig. 8 illustrates the effects of φ on the instantaneous Nu_{avg} when Re = 100, α = 0.5. The figure shows that the smaller values of φ gives smaller values of the amplitude of the instantaneous Nu_{avg}, while the higher the value of φ gives higher values of the amplitude of the instantaneous Nu_{avg}, and steady regime is observed.

While Fig. 9 illustrates the effect of φ on Nu_s at Re=100 and α = 0.5 when t=100. It is obvious that increasing φ increases Nu_s which reaches its maximum value at θ≅180° (corresponds to the front stagnation point) and it reaches its minimum value at θ≅45°, θ≅315°.

Fig. 10 illustrates the effects of φ on the streamlines contour when Re=100 and α=0.5 when t=100. From the figure one can note that φ has significant effects on the streamlines where increasing φ increases Re which is considered a dominant variable that affects the streamlines. Increasing φ increases the separation at the front stagnation point θ≅180° on the cylinder surface which in turn increases Nu_s at this point. The formation of the vortices behind the cylinder is also affected by increasing φ. This figure also indicates that the magnitude of the maximum negative velocity in recirculation zone is increased by any increment in φ and Re.

Fig. 11 illustrates the effect of φ on the temperature contours when Re = 100 and α = 0.5 when t=100. From the temperature distribution contours, it can be concluded that the temperature contours are steeper in the near-wake region with increasing φ as increasing φ in turn increases Reynolds number. This confirms that higher nanoparticles volume fraction (higher Reynolds number) resulting in higher temperature gradient, leading to an enhanced heat transfer from the cylinder. Thus, due to higher temperature gradient, temperature contours are much denser near the front surface of the cylinder. It can also be seen that the nanoliquid gives higher heat transfer rate from the cylinder than base fluid.

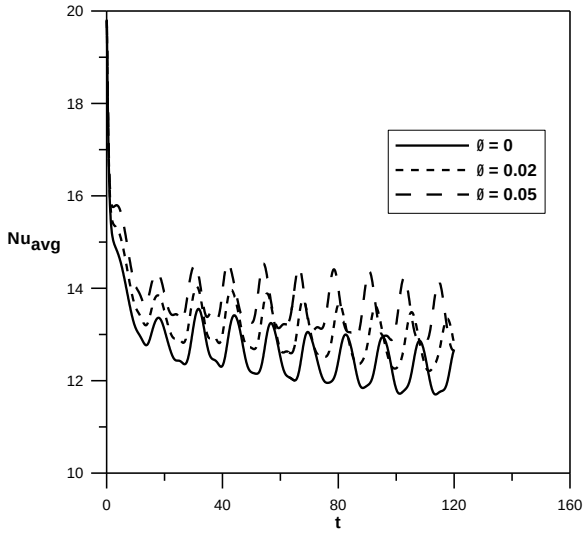

Figure 8- The effect of φ on the instantaneous Nu_{avg} when Re=100, α = 0.5, and t=100.

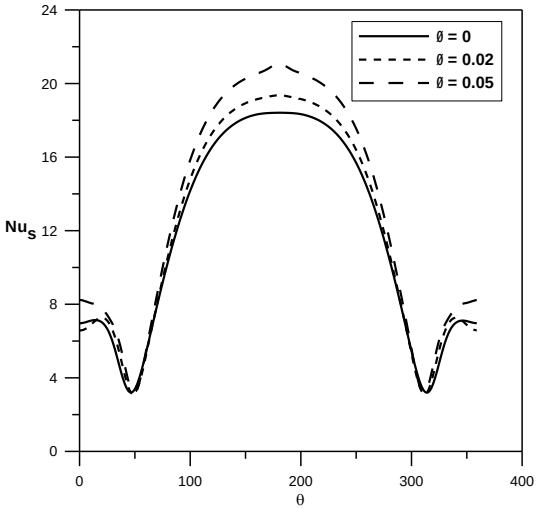

Figure 9- The effects of φ on Nu_s when Re=100, α = 0.5, and t=100.

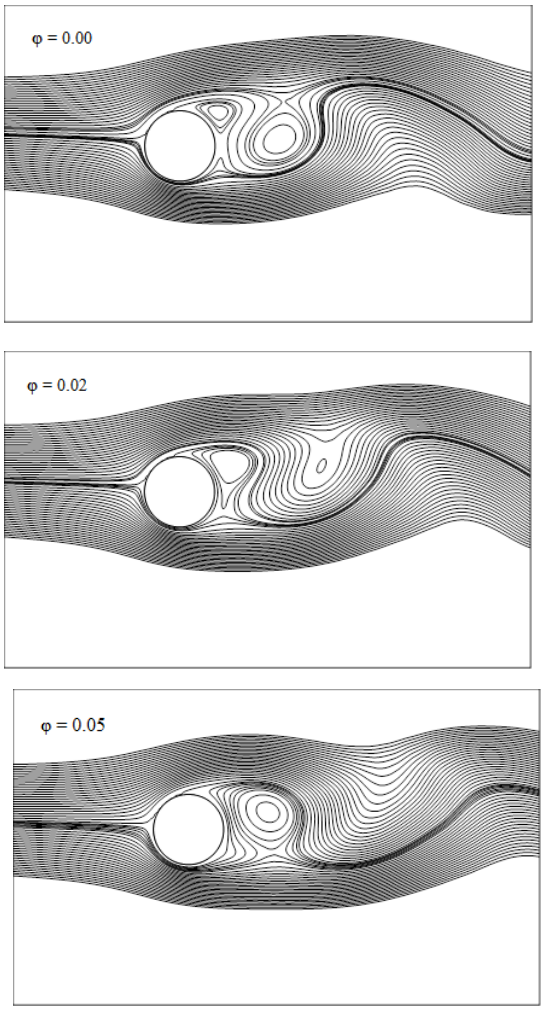

Figure 10- The effect of φ on the streamlines when Re=100, α=0.5, and t=100.

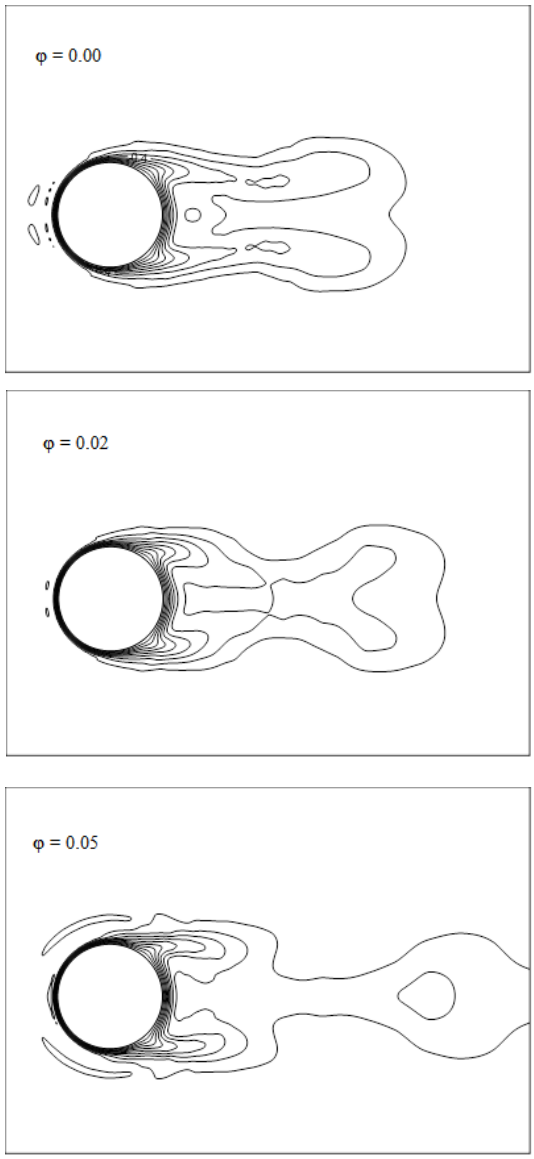

Figure 11- The effect of φ on the temperature contours when Re=100, α=0.5, and t=100.

To investigate the effects of α on different flow variables, one can compare between the values of: St, Nu_{avg}, C_D and C_L in table 5 where α=0.5 and the corresponding values in table 6 where α=1.

It is clear that increasing α decreases Nu_{avg},, C_L, and C_D is decreased by increasing α. Fig. 12 illustrates the effects of φ on the instantaneous Nu_{avg} when Re = 100, α = 1 when t = 100. The main effect of increasing α is decreasing Nu_{avg} at any value φ, also secondary peak values of Nu are increased by increasing φ.

Table 6- The effects of φ on St, Nu_{avg}, and C_D and C_L at Re=100, α = 1.

φ	Nu_{avg}	C_L	C_D
0.00	11.40464	-1.349646	1.5402
0.01	11.44148	-1.181404	1.511894
0.02	11.66776	-1.05152	1.504815
0.03	12.29016	-.9882069	1.516519
0.05	13.50488	-1.038123	1.569275

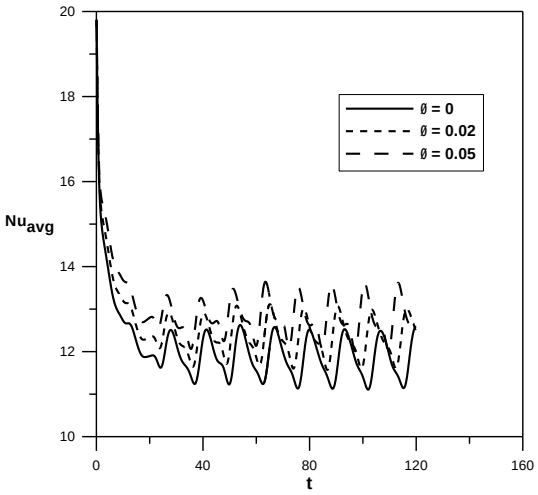

Figure 12- The effect of φ on the instantaneous Nu_{avg} when Re=100 and α = 1, and t=100.

Fig. 13 illustrates the effect of φ on the Nu_s when Re = 100, α = 1, and t = 100. Comparing this figure with Fig. 9 when α = 0.5, no significant change in the maximum of Nu_s for φ = 0, φ = 0.02 but increase in maximum of Nu_s at φ = 0.05 is significant. At θ = 0°, significant decrease in Nu_s at α = 1 compared with the same value at α = 0.5.

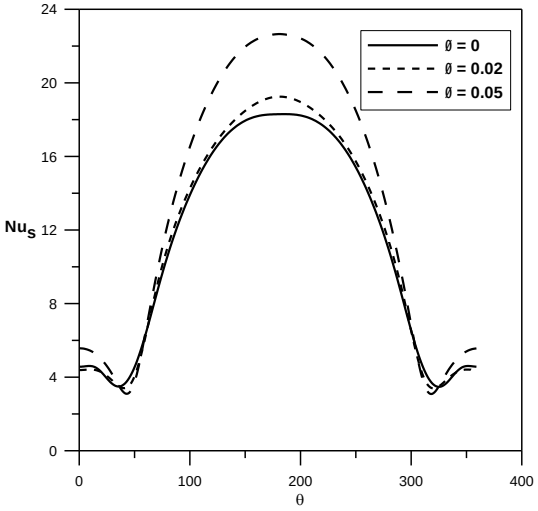

Figure 13- The effects of φ on Nu_s when Re=100 and α = 1, and t=100.

Fig. 14 illustrates the effects of φ on the streamlines patterns when Re=100 and α=1 for: φ = 0, φ = 0.02, φ = 0.05. It is to be noted that increasing α enhances the separation of the flow at the front stagnation point where θ=180° this clarify the increase in Nu_s therefore. Also, increasing α improves the detachment of the stream lines close to the cylinder surface at θ≅320° and θ≅45°. This may clarify the decrease in both Nu_{avg} and Nu_s due to increasing the speed ratio α.

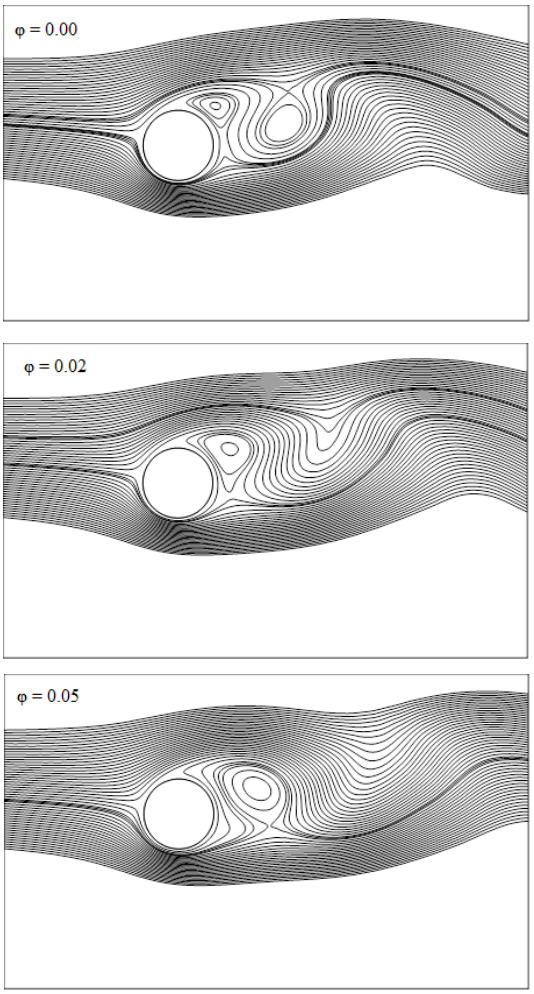

Figure 14- The effect of φ on the streamlines when Re=100, α=1, and t=100.

Fig. 15 illustrates the effects of φ on temperature contours when Re=100 and α = 1. It can be concluded from both Fig. 15 and Fig. 11 that temperature contours are almost symmetric around θ=0 (for small values of speed ratio). Also, increasing α tends to increase the volume of the isolated fluid rotating around the cylinder (from comparison between Fig. 11 and Fig. 14), this can clarify that the

temperature contours are not much denser near the front surface of the cylinder if compared with Fig. 11, which in turn leads to that the overall heat transfer coefficient tends to decrease as the speed ratio increases.

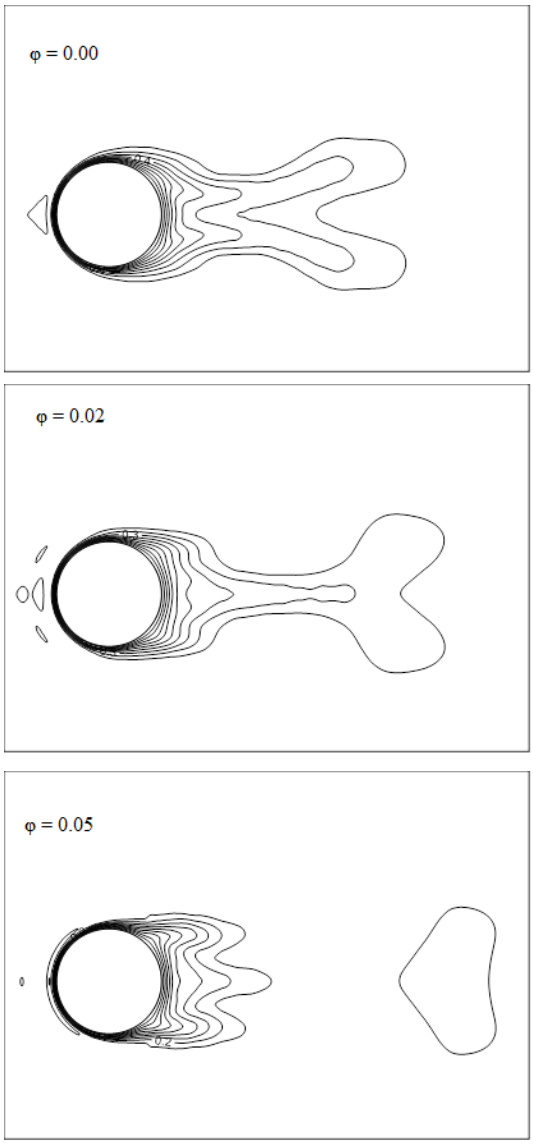

Figure 15- The effect of φ on the temperature contours when Re=100, α=1 and t=100.

Conclusions

From the present research, one can deduce the following results for the unsteady flow of viscous fluids under Stokes conditions:

1. Increasing nanoparticles volume fraction φ results in higher temperature gradient, leading to an enhanced heat transfer from the cylinder. Thus, due to higher temperature gradient, temperature contours are much denser near the front surface of the cylinder, generally increases heat transfer coefficient (Nusselt number).
2. Increasing nanoparticles volume fraction φ increases drag coefficient for the case of stationary cylinder. Increasing φ decreases drag coefficient for low speed ratios, has no significant effect on lift coefficient, and has a slight increasing effect on Strouhal number.
3. Increasing speed ratio α tends to increase the volume of the isolated fluid rotating around the cylinder which make the temperature contours are not much denser near the front surface of the cylinder which in turn leads to that the overall heat transfer coefficient tends to decrease as the speed ratio increases.
4. Increasing speed ratio α decreases both lift and drag coefficient (for low speed ratios), also Strouhal number is decreased.

Recommendations for Future Work

1. Optimization of both Nusselt number and drag coefficient has vital importance for optimum objectives of the forced convection from a steadily rotating cylinder in a cross flow of a nanoliquid. Optimization can be accomplished by using various methods for the main variables (speed ratio, Reynolds number, and nanoparticles volume fraction) that affect the objectives of the problem under investigation and it might be done to develop the present problem.
2. Comparison between cylinders with circle cross section and cylinders with elliptic cross section might be done for the problem under investigation.
3. Stability analysis is required to validate and improve the deduced results of the system under investigation and any corresponding systems.
4. Dynamic analysis can be done considering the magneto-nanoliquid property.

Appendix

$$S_o = \sum_{n=1}^{N}\left[\frac{\partial}{\partial\xi}(F_n\, g_n) - \frac{\partial}{\partial\xi}(f_n\, G_n)\right] \quad \text{(A-1)}$$

$$S_{n1} = \sum_{m=1}^{N}\frac{\partial g_m}{\partial\xi}\left[k\, f_k - J\, f_J\right] + \frac{\partial G_m}{\partial\xi}\left[k\, F_k - (m-n)f_J\right] + \sum_{m=1}^{N} m\, g_m\left[\frac{\partial f_k}{\partial\xi} - sgn\,(m-n)\frac{\partial f_J}{\partial\xi}\right] + m\, G_m\left[\frac{\partial F_k}{\partial\xi} - \frac{\partial F_J}{\partial\xi}\right] \quad \text{(A-2)}$$

$$S_{n2} = \sum_{m=1}^{N}\frac{\partial g_m}{\partial\xi}\left[k\, F_k + (m-n)F_J\right] - \frac{\partial G_m}{\partial\xi}\left[k\, f_k + J\, f_J\right] + \sum_{m=1}^{N} m\, g_m\left[\frac{\partial F_k}{\partial\xi} + \frac{\partial F_J}{\partial\xi}\right] - m\, G_m\left[\frac{\partial f_k}{\partial\xi} + sgn\,(m-n)\frac{\partial f_J}{\partial\xi}\right] \quad \text{(A-3)}$$

$$Z_o = \sum_{n=1}^{N} n\left[\frac{\partial}{\partial\xi}(F_n\, h_n) - \frac{\partial}{\partial\xi}(f_n\, H_n)\right] \quad \text{(A-4)}$$

$$Z_{n1} = \sum_{m=1}^{N}\frac{\partial H_m}{\partial\xi}\left[k\, F_k - (m-n)F_J\right] + \frac{\partial h_m}{\partial\xi}\left[k\, f_k - J\, f_J\right] + \sum_{m=1}^{N} m\, H_m\left[\frac{\partial F_k}{\partial\xi} - \frac{\partial F_J}{\partial\xi}\right] + m\, h_m\left[\frac{\partial f_k}{\partial\xi} - sgn\,(m-n)\frac{\partial f_J}{\partial\xi}\right] \quad \text{(A-5)}$$

$$Z_{n2} = -\sum_{m=1}^{N}\frac{\partial H_m}{\partial\xi}\left[k\, f_k + J\, f_J\right] + \frac{\partial h_m}{\partial\xi}\left[k\, F_k + (m-n)F_J\right] - \sum_{m=1}^{N} m\, H_m\left[\frac{\partial f_k}{\partial\xi} + sgn\,(m-n)\frac{\partial f_J}{\partial\xi}\right] + m\, h_m\left[\frac{\partial F_k}{\partial\xi} + \frac{\partial F_J}{\partial\xi}\right] \quad \text{(A-6)}$$

List of symbols

English Letters

R	Cylinder radius [m]
C_p	Specific heat at constant pressure [J/kg.°K]
h,$\bar{h}$	Local and average heat transfer coefficients
K	Fluid Thermal conductivity [W/m.°K]
Nu	Nusselt number
Nu_{avg}	Average Nusselt number
Nu_s	Surface Nusselt number
U_r,U_θ	Velocity components of fluid in polar coordinates
V	Uniform fluid stream velocity [m/s]
U_S	Cylinder velocity [m/s]
P	Pressure distribution of the fluid [Pa]
P*	Normalized Pressure distribution of the fluid
Pr	Prandtl number
Re	Reynolds number
r	Radial coordinate [m]
$r^/$	Dimensionless radial coordinate
T	Fluid temperature [°K]
T_∞	Uniform fluid stream temperature [°K]
T_S	Cylinder surface temperature [°K]
t	Time [s]
$t^/$	Dimensionless time
St	Strouhal number
C_D	Drag coefficient
C_{DP}	Pressure Drag coefficient
C_{DF}	Friction Drag coefficient
C_L	Lift coefficient
C_{LP}	Pressure Lift coefficient
C_{LF}	Friction Lift coefficient

Greek letters

Ψ	Stream function
Ω	Vorticity function
ϕ	Dimensionless fluid temperature
ξ	Dimensionless logarithmic coordinate
ρ	Density [kg/m^3]
μ	Dynamic viscosity [kg/m.s}
θ	Angular coordinate
φ	Nanoparticles volume fraction
α	Speed ratio
ν	Kinematic viscosity [m^2/s]

Subscripts

f	Fluid
nf	Nanoliquid
p	Particle
s	Surface of the cylinder
∞	Finite distance

References

[1] I. Khan, K. Saeed, I. Khan, Nanoparticles: applications and toxicities, Arab. J. ،Properties .931–Chem. 12 (2019) 908 .https://doi.org/10.1016/j.arabjc.2017.05.011

[2] nanoparticle | Definition, Size Range, & Applications | Britannica, (n.d.). https://www.britannica.com/science/nanoparticl .(2021 ،e (accessed July 26

[3] S. Horikoshi, N. Serpone, Introduction to Nanoparticles, Microwaves Nanoparticle Synth. .24–Fundam. Appl. (2013) 1 .https://doi.org/10.1002/9783527648122.ch1

[4] Prandtl: The Magnus effect and windpowered Google Scholar, (n.d.). -ships scholar.google.com/scholar_lookup?title//:https powered -The magnus effect and wind= ships&journal=Naturwissenschaften&volume=1 -pages=93&3 publication_year=1925&author=Prandtl%&108 .(CL (accessed February 12, 20212

[5] dependent viscous flow past -S.C. Dennis, Time impulsively started rotating and translating an circular cylinder, J. Fluid Mech. 158 (1985) .488–447 .https://doi.org/10.1017/S0022112085002725

[6] H.M. Badr, S.C.R. Dennis, Laminar forced convection from a rotating cylinder, Int. J. Heat .264–253 (85Mass Transf. 28 (19 .4-90027(85)9310-https://doi.org/10.1016/0017

[7] D.B. Ingham, T. Tang, A numerical investigation into the steady flow past a rotating circular cylinder at low and intermediate Reynolds numbers, J. Comput. Phys. 87 (1990) -https://doi.org/10.1016/0021 .107–91 .R-90227(90)9991

[8] D. Stojković, M. Breuer, F. Durst, Effect of high rotation rates on the laminar flow around a –circular cylinder, Phys. Fluids. 14 (2002) 3160 .https://doi.org/10.1063/1.1492811 .3178

[9] hön, M. Breuer, F. Durst, On D. Stojković, P. Sc the new vortex shedding mode past a rotating –circular cylinder, Phys. Fluids. 15 (2003) 1257 .https://doi.org/10.1063/1.1562940 .1260

[10] S. Mittal, B. Kumar, Flow past a rotating .334–cylinder, J. Fluid Mech. (2003) 303 .doi.org/10.1017/S0022112002002938//:https

[11] S. Sanitjai, R.J. Goldstein, Forced convection heat transfer from a circular cylinder in crossflow to air and liquids, Int. J. Heat Mass .4805–Transf. 47 (2004) 4795 https://doi.org/10.1016/j.ijheatmasstransfer.20 .04.05.012

[12] K. Abdella, for Forced Convection Heat Flow Past a Rotating -Transfer from a Shear .527–Cylinder, 2 (2008) 497

[13] S.B. Paramane, A. Sharma, Numerical investigation of heat and fluid flow across a nstant rotating circular cylinder maintained at co D laminar flow regime, Int. J. -temperature in 2 .3216–Heat Mass Transf. 52 (2009) 3205 https://doi.org/10.1016/j.ijheatmasstransfer.200 .8.12.031

[14] S.B. Paramane, A. Sharma, Heat and fluid flow across a rotating cylinder dissipating uniform lux in 2D laminar flow regime, Int. J. Heat heat f .4683–Mass Transf. 53 (2010) 4672 https://doi.org/10.1016/j.ijheatmasstransfer.201 .0.06.026

[15] R. Bouakkaz, F. Salhi, Y. Khelili, M. Quazzazi, K. Talbi, Unconfined laminar nanofluid flow d a rotating circular and heat transfer aroun cylinder in the steady regime, Arch. .20–Thermodyn. 38 (2017) 3 .0008-2017-https://doi.org/10.1515/aoter

[16] Y. Khelili, A. Allali, R. Bouakkaz, Numerical investigation of forced convective heat transfer der utilizing around a solid circular cylin nanofluid in unsteady regime, Eng. Rev. 39 .269–261 (2019) .https://doi.org/10.30765/er.39.3.07

[17] S. Hussain, M. Jamal, S.E. Ahmed, Hydrodynamic forces and heat transfer of nanofluid forced convection flow around a finite element method: rotating cylinder using The impact of nanoparticles, Int. Commun. Heat Mass Transf. 108 (2019) 104310. https://doi.org/10.1016/j.icheatmasstransfer.201 .9.104310

[18] K. Korib, N. Ihaddadene, R. Bouakkaz, Y. Khelili, Numerical simulation of forced of nanofluid aroUnd a circular convection .16–cylinder, Arch. Thermodyn. 40 (2019) 3 .https://doi.org/10.24425/ather.2019.129539

[19] S.J.D. D'Alessio, S.C.R. Dennis, Steady laminar forced convection from an elliptic .193–cylinder, J. Eng. Math. 29 (1995) 181 .doi.org/10.1007/BF00051742//:https

[20] D. Kumar, A.K. Sahu, EasyChair Preprint Forced Convection Heat Transfer from a Rotating Elliptic Cylinder in the Laminar Flow xxxx Forced -xx-Regime IHMTC2019 convection Heat Transfer from a Rotating he Laminar Flow Regime, Elliptic Cylinder in t .(2021)

[21] S.A. Patel, R.P. Chhabra, Forced convection from an inclined elliptical cylinder with constant heat flux: Effect of Prandtl number, .394–Lect. Notes Mech. Eng. (2017) 385 .37_4-2743-322-81-https://doi.org/10.1007/978

[22] B.C. Pak, Y.I. Cho, Hydrodynamic and heat transfer study of dispersed fluids with

submicron metallic oxide particles, Exp. Heat .170–Transf. 11 (1998) 151 .https://doi.org/10.1080/08916159808946559

[23] W. Yu, S.U.S. Choi, The role of interfacial in the enhanced thermal conductivity of layers Crosser -nanofluids: A renovated Hamilton .361–model, J. Nanoparticle Res. 6 (2004) 355 .7-2601-004-https://doi.org/10.1007/s11051

[24] H.C. Brinkman, The viscosity of concentrated Phys. 20 .suspensions and solutions, J. Chem .https://doi.org/10.1063/1.1700493 .571 (1952)

[25] M. Aliofkhazraei, Handbook of nanoparticles, -15338-319-3-https://doi.org/10.1007/978 .2015 .4

[26] A.A. Hashim, Smart nanoparticles technology / .monograph., 2012

[27] eat convection F.M. Mahfouz, H.M. Badr, H from a cylinder performing steady rotation or Part I: Steady rotation, Heat -rotary oscillation Mass Transf. Und Stoffuebertragung. 34 (1999) .373–365 .https://doi.org/10.1007/s002310050271

[28] dependent viscous flow past-S.C. Dennis, Time an impulsively started rotating and translating circular cylinder, J. Fluid Mech. 158 (1985) .488–447 .https://doi.org/10.1017/S0022112085002725

[29] F.M. Mahfouz, H.M. Badr, Flow structure in the wake of a rotationally oscillating cylinder, J. .301–Trans. ASME. 122 (2000) 290 .Fluids Eng .https://doi.org/10.1115/1.483257

[30] F.M. Mahfouz, H.M. Badr, Forced convection from a rotationally oscillating cylinder placed in a uniform stream, Int. J. Heat Mass Transf. 43 .3104–3093 (2000) -00326(99)9310-S0017/https://doi.org/10.1016 .9

[31] T.P. Loc, Numerical analysis of unsteady secondary vortices generated by an impulsively started circular cylinder, J. Fluid Mech. 100 .128–111 (1980) .https://doi.org/10.1017/S0022112080001036

[32] luence of M. Coutanceau, C. Menard, Inf wake development behind -rotation on the near an impulsively started circular cylinder, J. Fluid .446–Mech. 158 (1985) 399 .https://doi.org/10.1017/S0022112085002713

[33] E.F.R. A.R.C.Sc., L.F.G.S.B.A. A.R.C.Sc., LIII. eddies generated by the On the frequency of the motion of circular cylinders through a fluid, Https://Doi.Org/10.1080/14786442508634628. .511–509 (2009) 49 .https://doi.org/10.1080/14786442508634628

[34] C.H. Cheng, J.L. Hong, W. Aung, Numerical nvective heat on effect on co-prediction of lock transfer from a transversely oscillating circular cylinder, Int. J. Heat Mass Transf. 40 (1997) -https://doi.org/10.1016/S0017 .1834–1825 .4-00255(96)9310

[35] H. Kramers, Heat transfer from spheres to .80–flowing media, Physica. 12 (1946) 61 -80024(46)8914-https://doi.org/10.1016/S0031 .7

[36] V.T. Morgan, The Overall Convective Heat Transfer from Smooth Circular Cylinders, Adv. .264–Heat Transf. 11 (1975) 199 -70075(08)2717-https://doi.org/10.1016/S0065 .3

[37] Study of P.C. Jain, B.S. Goel, A Numerical Unsteady Laminar Forced Convection From a Circular Cylinder, J. Heat Transfer. 98 (1976) .https://doi.org/10.1115/1.3450537 .307–303

[38] state numerical solution of -R.A. Ahmad, Steady stokes and energy equations around a -the navier linder at moderate reynolds horizontal cy numbers from 100 to 500, Heat Transf. Eng. 17 .81–31 (1996) .https://doi.org/10.1080/01457639608939866

[39] Heat and Mass Transfer in Turbulent Separated Google Books, (n.d.). -Flows _https://books.google.com.eg/books/about/Heat and_Mass_Transfer_in_Turbulent_Sepa.html?id U7qVNwAACAAJ&redir_esc=y (accessed = .(August 27, 2021

[40] induced oscillations: A -G. V. Parkinson, Vortex selective review, J. Appl. Mech. Trans. ASME. .453 (1980) 47 .https://doi.org/10.1115/1.3153698

[41] oshko, On the Development of Turbulent A. R Wakes from Vortex Streets, (1954). https://resolver.caltech.edu/CaltechAUTHORS: .(ROSnacarpt1191 (accessed February 26, 2021